Theoretical Investigation of Electrocyclic Ring Closure Reactions in Bis(aryloxy)bis(η^2-iminoacyl)zirconium and Isoelectronic Complexes

Jon H. Hardesty, Thomas A. Albright,* and Samia Kahlal

Department of Chemistry, University of Houston, Houston, Texas 77204-5641

Received January 25, 2000

A theoretical investigation of the ligand coupling reactions in the isoelectronic series $(HO)_2Zr(\eta^2\text{-}CHO)_2$, **9**, $(HO)_2Zr(\eta^2\text{-}CHNH)_2$, **10**, and $(HO)_2W(\eta^2\text{-}HCCH)_2$, **11**, has been carried out at the hybrid density functional level of theory. The structures of **9**−**11** and their experimentally observed analogues are isolobal to 20-valence-electron species of the form $Cp_2M(\eta^2\text{-}L)_2$ which have previously been shown to have a $Cp_2M(\eta^2\text{-}L)(\eta^1\text{-}L)$ structure. Our calculations show that the bent geometry of the $(HO)_2M$ fragment greatly reduces metal−oxygen π-overlap in two of the four metal−oxygen π-interactions, which allows the $(HO)_2M$ metal fragment to bind two ligands in an η^2-fashion without exceeding coordinative saturation at the metal. The mechanism of formyl, iminoformyl, and acetylene coupling in **9**−**11** follows a path in which the coordinated ligands undertake a scissors-like motion that pulls the carbon atoms away from the metal and toward one another. In agreement with experimental observations, formyl coupling in **9** occurs more rapidly ($\Delta E^{\ddagger} = 14.0$ kcal/mol) than iminoformyl coupling in **10** ($\Delta E^{\ddagger} = 19.4$ kcal/mol), which, in turn, occurs more rapidly than acetylene coupling in **11**. This latter reaction was found to be formally symmetry forbidden. We attribute this relative order of reactivity to the steadily decreasing electronegativity of the η^2-bound ligands that is manifested in two ways in the electronic structures of **9**−**11** as they undergo ligand coupling. Overall the conversions of **9** to enediolate **12**, **10** to enediamide **13**, and **11** to metallacyclopentatriene **14** are strongly exothermic by 58.1, 45.4, and 21.6 kcal/mol, respectively.

Introduction

Dialkyl metallocene complexes of the early d-block and actinide metals are characteristically known to undergo CO activation via the formation of enediolate complexes.[1] Two pathways have been proposed in the literature to account for this transformation depending upon the nature of the metal center, both of which are shown in Scheme 1. The initial step in both cases is the insertion of 1 equiv of carbon monoxide to generate a monoacyl complex bearing the kinetically preferred η^2-O-outside conformation via the well-known Erker mechanism.[2] In the case of actinide metallocene systems, a second such insertion is proposed to occur, resulting in the formation of a 20-valence-electron bis-(η^2-acyl) species, **1**, in which the acyl ligands adopt a coplanar coordination geometry. Coupling of the acyl ligands in **1** occurs after the acyl moieties rotate in a conrotatory fashion about their coordination axes with the metal; a

Scheme 1

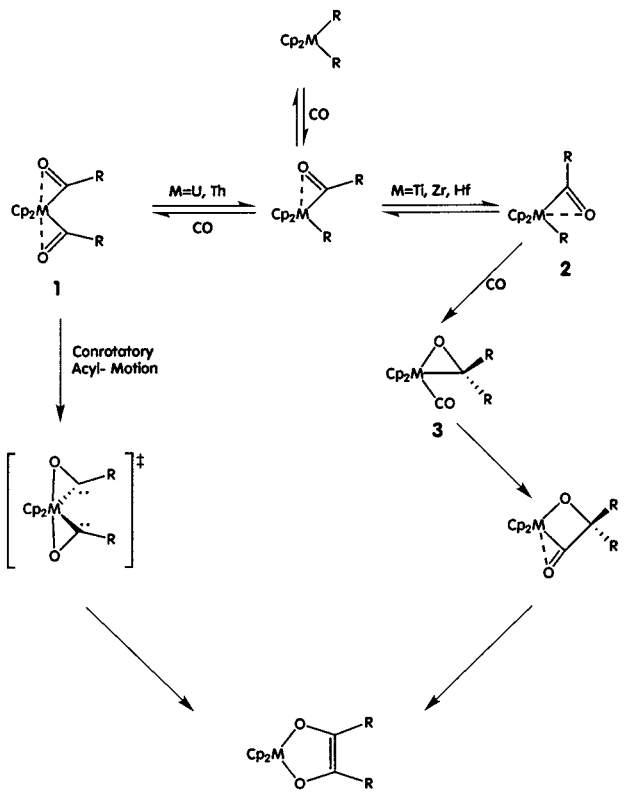

(1) (a) Crabtree, R. H. *The Organometallic Chemistry of the Transition Metals*; Wiley: New York, 1994. (b) Durfee, L. D.; Rothwell, I. P. *Chem. Rev.* **1988**, *88*, 1059. (c) Manriquez, J. M.; McAlister, D. R.; Sanner, R. D.; Bercaw, J. E. *J. Am. Chem. Soc.* **1976**, *98*, 6733. (d) Manriquez, J. M.; McAlister, D. R.; Sanner, R. D.; Bercaw, J. E. *J. Am. Chem. Soc.* **1978**, *100*, 2716. (e) Manriquez, J. M.; Fagan, P. J.; Marks, T. J.; Day, C. S.; Day, V. W. *J. Am. Chem. Soc.* **1978**, *100*, 7112. (f) Evans, W. J.; Grate, J. W.; Doedens R. J. *J. Am. Chem. Soc.* **1985**, *107*, 1671.

(2) (a) Erker, G. *Acc. Chem. Res.* **1984**, *17*, 103. (b) Tatsumi, K.; Nakamura, A.; Hofmann, P. Stauffert, P.; Hoffmann, R. *J. Am. Chem. Soc.* **1985**, *107*, 4440.

10.1021/om000064i CCC: $19.00
Publication on Web 09/07/2000

more direct in-plane coupling pathway was found to be symmetry forbidden.[3a] A theoretical investigation[3a] of this mechanism undertaken at the extended Hückel level revealed that the ability of **1** to adopt a coplanar arrangement of the acyl ligands with a formal 20-valence-electron count at the metal was due to the participation of an empty, low lying f-orbital. In the absence of energetically accessible f-functions, as in the group IV metallocene systems, the attainment of a 20-valence-electron count at the metal thermally disfavors the intermediacy of **1**.[3a,4] For these systems an alternative mechanism, shown on the right side of Scheme 1, has been proposed and theoretically investigated at the extended Hückel level.[4] In this pathway the initially formed mono(η^2-acyl) complex isomerizes to give the more thermodynamically stable η^2-O-inside conformer **2**. The η^2-acyl moiety then slips to an η^1-coordination mode and rotates by 90°. This allows the remaining metal-bound alkyl group to migrate to the acyl-carbon atom with assistance from the coordination of a second equivalent of carbon monoxide and results in the formation of η^2-ketone complex **3**. Subsequent insertion of the newly coordinated carbon monoxide ligand into the metal−carbon bond of the η^2-bound ketone, either followed or accompanied by alkyl migration, completes enediolate formation.

Complicating this cogent mechanistic picture was the report of Rothwell and co-workers[5] indicating that bis(aryloxy)zirconium dialkyl complexes readily insert alkyl-isocyanides (RNC) to generate bis(η^2-iminoacyl)-complexes **4**, as shown in eq 1. These isolable complexes

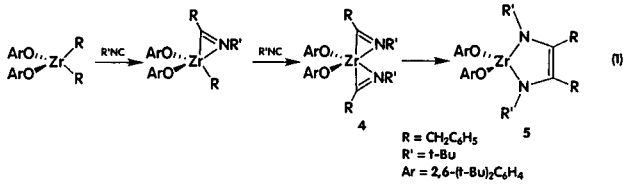

react further via iminoacyl coupling to generate enediamide complexes **5**. This result was a little surprising given that alkylisocyanides are isoelectronic with carbon monoxide and that linear alkoxide/aryloxide ligands are isolobal with η^5-Cp ligands,[6] making **4** an isolobal analogue of **1** that contains a group IV metal! We were also struck by a reactivity pattern noted by the authors[5] in which bis(η^2-iminoacyl) complexes, **4**, could be isolated and subsequently prompted to undergo ligand coupling, whereas no intermediate species analogous to **4** could be observed in the corresponding reaction between $(ArO)_2Zr(\eta^2\text{-}R'N{=}CR)(R)$ and CO leading to the eneamidolate complex **6**, shown in eq 2. This suggested

Scheme 2

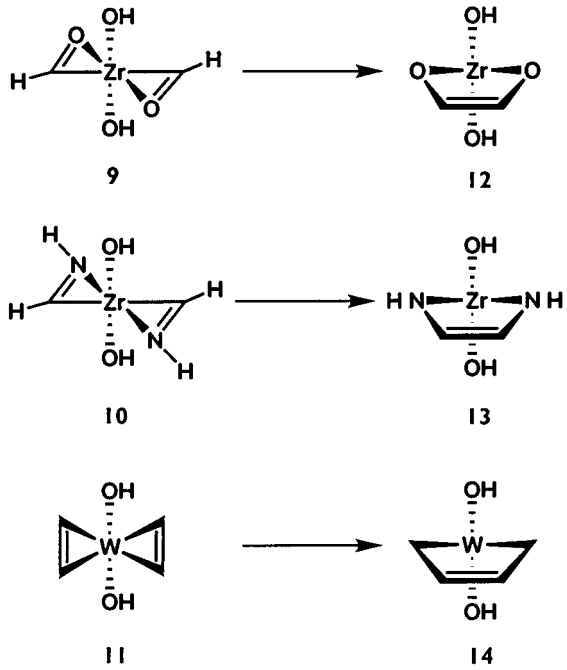

to us that the substitution of a more electronegative oxygen atom for an NR′ moiety was directly influencing the magnitude of the activation energy of the ligand coupling step. Rothwell and co-workers[7] also reported the difficulty with which $(2,6\text{-}(C_6H_5)_2C_6H_3O)_2W(\eta^2\text{-}C_2Et_2)_2$, **7**, yet another isoelectronic counterpart to **4**, underwent acetylene coupling to generate the tungstacyclopentatriene **8**, as shown in eq 3.

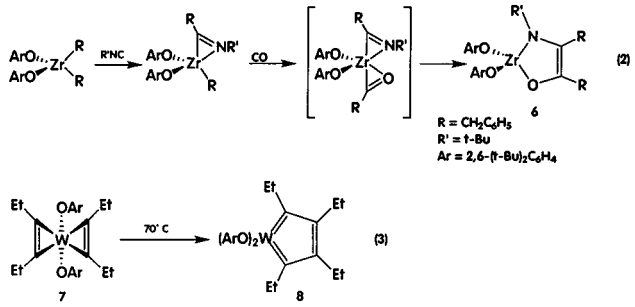

Given this combination of novel structural characteristics and reactivity trends, we chose to undertake a theoretical investigation of the mechanism of ligand coupling in these aryloxide systems in an effort to understand how they differ from the actinide and group IV metallocene systems studied at the extended Hückel level. To simplify the computational complexity of this investigation, we have carried out our calculations on the three model reactions shown in Scheme 2, in which we have substituted hydroxide moieties for the aryloxide ligands present in Rothwell's complexes. Moreover, in an effort to maintain a maximum amount of symmetry, we chose to model the effects of oxygen substitution on the reaction leading to the formation of **6** by the coupling of two formyl ligands. While this particular reaction has not been observed to occur in the presence of the

(3) (a) Tatsumi, K.; Nakamura, A.; Hofmann, P.; Hoffmann, R.; Moloy, K. G.; Marks, T. J. *J. Am. Chem. Soc.* **1986**, *108*, 4467. (b) Fagan, P. J.; Manriquez, J. M.; Vollmer, S. H.; Day, C. S.; Day, V. W.; Marks, T. J. *J. Am. Chem. Soc.* **1981**, *103*, 2206.

(4) Hofmann, P.; Stauffert, P.; Frede, M.; Tatsumi, K. *Chem. Ber.* **1989**, *122*, 1559.

(5) (a) McMullen, A. K.; Rothwell, I. P.; Huffman, J. C. *J. Am. Chem. Soc.* **1985**, *107*, 1072. (b) Chamberlain, L. R.; Durfee, L. D.; Fanwick, P. E.; Kobriger, L.; Latesky, S. L.; McMullen, A. K.; Rothwell, I. P.; Folting, K.; Huffman, J. C.; Streib, W. E.; Wang, R. *J. Am. Chem. Soc.* **1987**, *109*, 390.

(6) Based upon the Cp-imido analogy of R. R. Schrock, V. C. Gibson, J. C. Green, and co-workers. See: Glueck, D. S.; Green, J. C.; Michelman, R. I.; Wright, I. N. *Organometallics* **1992**, *11*, 4221, and references therein.

(7) (a) Kerschner, J. L.; Fanwick, P. E.; Rothwell, I. P. *J. Am. Chem. Soc.* **1988**, *110*, 8235. (b) Kriley, C. E.; Kerschner, J. L.; Fanwick, P. E.; Rothwell, I. P. *Organometallics* **1993**, *12*, 2051.

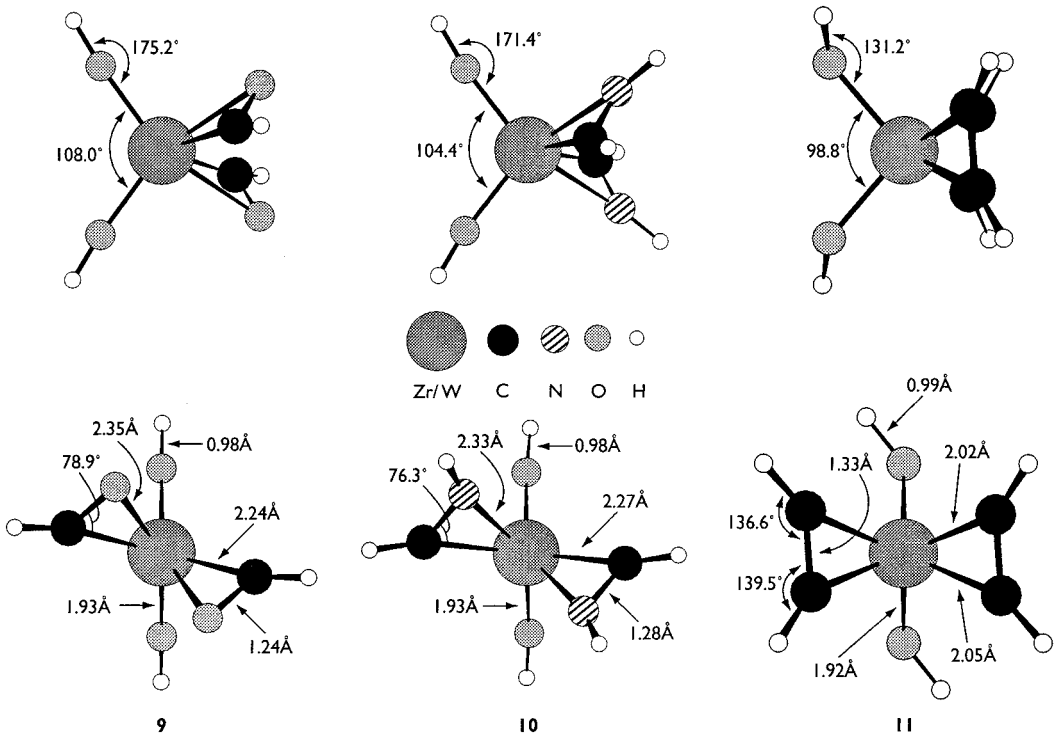

Figure 1. B3LYP-optimized geometries of $(HO)_2Zr(\eta^2\text{-}CHO)_2$, **9**, $(HO)_2Zr(\eta^2\text{-}HNCH)_2$, **10**, and $(HO)_2W(\eta^2\text{-}HCCH)_2$, **11**.

aryloxide ligand set, we expect the results obtained from this model reaction to reveal the electronic effects responsible for the observed reactivity trends when carbon monoxide is substituted for 1 equiv of alkylisocyanide.

Computational Details

All structures reported herein were optimized at the hybrid density functional theory (DFT) level using Becke's three-parameter hybrid exchange−correlation functional[8] containing the nonlocal gradient correction of Lee, Yang, and Parr[9] (Becke3LYP) within the Gaussian94[10] program package. All optimized structures were confirmed as minima or transition states by calculation of numerical vibrational frequencies, and all reported energies are corrected for the effects of zero-point vibrational energy. A collection of Cartesian coordinates and total energies for all the molecules reported in this paper are available from the authors upon request. Basis sets for the Zr and W atoms utilized the effective core potentials of Hay and Wadt[11] with the associated double-ζ valence basis functions. For both metals the most diffuse d-function of the inner d-type GTO was decontracted, resulting in bases of the form (441/2111/211) for Zr and (441/2111/111) for W. All geometric optimizations were carried out with standard 6-31G*[12] basis sets on C, N, and O atoms of the acetylene, formyl, and iminoformyl ligands, and the remaining O and all H atoms were described by standard 3-21G[13] basis functions. Single-point calculations were carried out for the stationary points with a 6-31G* basis on all ligand atoms, and f-functions[14] were added to the transition metals. The relative energies here are taken from these calculations.

Extended Hückel calculations[15] were carried out using the modified Wolfsberg-Helmholtz approximation.[16] The parameters used in these calculations are taken from the literature.[17]

Results and Discussion

The Formyl, Iminoformyl, and Acetylene Complexes. Our B3LYP-optimized geometries of **9** and **10** are shown in Figure 1 with important bond distances and angles. Both structures possess pseudotetrahedral geometries of C_2 symmetry with the η^2-bound ligands in both species oriented in a head-to-tail fashion with respect to one another, matching the general structural characteristics observed in **4**.[5] Furthermore, the dihapto ligands are rotated about their coordination axes with the metal placing the more electronegative O and NH moieties "inside" the carbon atoms, reflecting the thermodynamic preference η^2-acyl ligands have for adopting an O-inside conformation in group IV metallocene complexes.[2] The formyl ligands in **9** exhibit the geometric characteristics typically observed in η^2-bound acyl ligands,[1b] namely, a short Zr−C σ-bond (2.24 Å), a considerably longer Zr−O bond (2.35 Å) that reflects the

(8) Becke, A. D. *J. Chem. Phys.* **1993**, *98*, 5648.
(9) Lee, C.; Yang, W.; Parr, R. G. *Phys. Rev. B* **1988**, *37*, 785.
(10) Frisch, M. J.; Trucks, G. W.; Schlegel, H. B.; Gill, P. M. W.; Johnson, B. G.; Robb, M. A.; Cheeseman, J. R.; Kieth, T.; Petersson, G. A.; Montgomery, J. A.; Raghavachari, K.; Al-Laham, M. A.; Zakrzewski, V. G.; Ortiz, J. V.; Foresman, J. B.; Cioslowski, J.; Stefanov, B. B.; Nanayakkara, A.; Challacombe, M.; Peng, C. Y.; Ayala, P. Y.; Chen, W.; Wong, M. W.; Andres, J. L.; Replogle, E. S.; Gomperts, R.; Martin, R. L.; Fox, D. J.; Binkley, J. S.; DeFrees, D. J.; Baker, J.; Stewart, J. P.; Head-Gordon, M.; Gonzalez, C.; Pople, J. A. *Gaussian 94, Revision B.1*; Gaussian, Inc.: Pittsburgh, PA, 1995.
(11) Hay, P. J.; Wadt, W. R. *J. Chem. Phys.* **1985**, *82*, 299.
(12) Francl, M. M.; Pietro, W. J.; Hehre, W. J.; Binkley, J. S.; Gordon, M. S.; DeFrees, D. J.; Pople, J. A. *J. Chem. Phys.* **1982**, *77*, 3654.
(13) (a) Binkley, J. S.; Pople, J. A.; Hehre, W. J. *J. Am. Chem. Soc.* **1980**, *102*, 939. (b) Gordon, M. S.; Binkley, J. S.; Pople, J. A.; Pietro, W. J.; Hehre, W. J. *J. Am. Chem. Soc.* **1983**, *104*, 2797.
(14) Ehlers, A. W.; Böhme, M.; Dapprich, S.; Gobbi, A.; Höllwarth, A.; Jonas, V.; Köhler, K. F.; Stegmann, R.; Veldkamp, A.; Frenking, G. *Chem. Phys. Lett.* **1993**, *208*, 111.
(15) Hoffmann, R. *J. Chem. Phys.* **1963**, *39*, 1397.
(16) Wolfsberg, M.; Helmholtz, L. *J. Chem. Phys.* **1952**, *20*, 837.
(17) (a) DuBois, D. L.; Hoffmann, R. *Nouv. J. Chim.* **1977**, *1*, 479. (b) Hoffman, D. M.; Hoffmann, R.; Fisel, C. R. *J. Am. Chem. Soc.* **1982**, *104*, 3858.

weakly coordinating nature of the carbonyl oxygen atom, and a highly acute Zr−C−O bond angle of 78.9°. These values compare quite favorably with the corresponding parameters of the η^2-acyl ligands found in $Cp_2Zr(\eta^2\text{-COMe})CH_3$,[18] **15**, $[Cp^*_2Zr(\eta^2\text{-COMe})(CO)]^+$,[19] **16**, and $Cp_2Zr(\eta^2\text{-COMe})(\mu\text{-OC})MoCp(CO)_2$,[20] **17**. Detailed comparison of the data reveals however that our calculated structure of **9** underrepresents the Zr−C bond lengths by 0.02−0.06 Å and the Zr−O bonds by 0.06−0.11 Å. Whether the longer calculated bond lengths in **9** are truly indicative of a bis-η^2-formyl complex or are an artifact of our choice of model chemistry is difficult to determine given that there are no experimentally characterized complexes of this type to compare with our calculations. The Zr−O−H bond angles of 175.2° in **9** indicate the presence of significant Zr−O multiple-bond character.

Similar structural characteristics are found in the optimized geometry of **10**, where the iminoformyl ligands possess relatively short Zr−C bonds (2.27 Å), longer Zr−N bonds (2.33 Å), and a highly acute Zr−C−N bond angle of 76.3°. The corresponding values observed by Rothwell and co-workers[5] in **4** were 2.23 Å for the Zr−C bond, 2.22 Å for the Zr−N bond, and 73.5° for the Zr−C−N bond angle. Thus, as in **9**, our theoretically calculated structure of **10** underrepresents the strength of the bonding interaction between the iminoformyl ligands and the Zr atom. Unlike in **9** above, both **4** and **10** possess a pair of η^2-bound ligands, leading us to suspect that our model complex overemphasizes electron donation to the metal originating from the hydroxyl ligands. Indeed we find nearly linear Zr−O−H bond angles in **10** (171.4°), suggesting a considerable amount of Zr−O multiple-bond character, and at 1.93 Å the Zr−O bond length in **10** supports this contention. Comparing this value with corresponding Zr−OAr bond distances in **4**[5] reveals that our calculated Zr−O bond is nearly 0.10 Å shorter than the experimentally observed values. Thus, the shorter distance modeled in **10** is most likely due to the absence of the sterically bulky 2,6-di-*tert*-butylphenyl groups in **4**. This deformation results in weaker Zr−O bonds and a more electron-deficient metal atom in **4**, compared to our model complex **10**, which is alleviated by stronger zirconium−(η^2-iminoacyl) interactions. Therefore, in our decision to simplify the computational complexity of our calculations by modeling the aryloxide ligands of **4** with hydroxyl moieties, we have underestimated the effect of steric bulk upon the electronic structure of these systems.

The B3LYP-optimized geometry of **11** is also shown in Figure 1. As in **9** and **10**, the optimized geometry of **11** possesses a pseudotetrahedral geometry of C_2 symmetry in which the acetylene ligands are rotated about their coordination axes with the W atom in a conrotatory fashion, although to a much smaller degree than what is seen for the formyl and iminoformyl ligands in **9** and **10**, respectively. The alkyne ligands in **11** are strongly bound, with W−C bond lengths (2.02 and 2.05 Å) that are typical of W−(η^2-acetylene) interactions.[21] The acetylenic C−C bond length is 0.03 Å longer than the mean value observed in alkyne ligands acting as four-electron donors,[21] and the acetylenic C−C−H bond angles are bent nearly 40° from linearity, also indicating considerable back-bonding. These values compare well with those observed in $(2,6\text{-}Ph_2C_6H_3O)_2W(\eta^2\text{-}C_2(C_2H_5)_2)_2$, **7**, by Rothwell and co-workers,[7b] where the W−C bond lengths ranged from 2.01 to 2.03 Å and the acetylenic C−C bonds measured 1.29−1.30 Å. At 1.92 Å the W−O bond distances in **11** are characteristic of terminal alkoxide−tungsten linkages.[21] The 131.2° W−O−H bond angles are ∼40° smaller than the corresponding angles in **9** and **10**, strongly implying that the oxygen atoms in **11** donate considerably less π-electron density to the central metal atom than the hydroxyl-oxygen atoms do in **9** and **10**. Since this same structural feature is observed in the X-ray crystal structure of **7**, where W−O−Ar bond angles measure 131.3° and 136.0°, it cannot be disregarded as an artifact of our calculation. We believe this feature is a result of the softer nature of the acetylene ligands in **11**, making them stronger donors than the relatively hard formyl and iminoformyl ligands in **9** and **10**. As a result, the tungsten atom in **11** is less dependent upon the hydroxyl moieties for electron density than the zirconium atoms are in **9** and **10**.

Given the structures of **9**−**11** and the isolobal relationship between the η^5-C_5H_5 ligand and the linear hydroxide ligand, one question immediately comes to mind. Namely, what makes the $(RO)_2M$ (M = Ti, Zr, Hf) metal fragment capable of binding two formyl, iminoformyl, or acetylene ligands in an η^2-fashion when the corresponding metallocene fragments apparently cannot? As we noted in the Introduction, complexes of the type **9**−**11** electronically correspond to 20-valence-electron species of the form $Cp_2M(\eta^2\text{-}COCH_3)_2$, which are known to be unstable in the absence of f-orbital participation to metal−ligand bonding.[3a] Thus, there must be some characteristic of the bisalkoxide/bishydroxide ligand set that fundamentally distinguishes it from the bis-Cp ligand set while maintaining the basic isolobal features between the two. Examination of the orbital interactions in the $[Zr(OH)_2]^{2+}$ metal fragment at the extended Hückel level reveals that the oxygen π-donor orbitals do not all overlap very strongly with the Zr d-set. This results in considerably less oxygen-to-zirconium electron donation than one might initially expect. The four fragment molecular orbitals involving π-overlap between the oxygen atoms and the zirconium atom in the $[Zr(OH)_2]^{2+}$ fragment of **9**, obtained at the B3LYP level, are shown in Figure 2. The lowest energy orbital, labeled a_1 in Figure 2, is largely an in-phase combination of oxygen-centered ($p_z + p_x$)-hybrids mixing in a bonding fashion with the $d_{z^2-x^2}$-orbital on zirconium. In this orbital Zr−O overlap is reasonably strong. The only detrimental factor appearing in a_1 is the significant electronegativity difference between oxygen and zirconium that keeps the fragment MO largely oxygen centered, a ubiquitous characteristic of all the orbitals shown in the Figure. The second highest energy π-or-

(18) Fachinetti, G.; Floriani, C.; Marchetti, F.; Merlino, S. *J. Chem. Soc., Chem. Commun.* **1976**, 522.
(19) Guo, Z.; Swenson, D. C.; Guram, A. S.; Jordan, R. F. *Organometallics* **1994**, *13*, 766.
(20) Marsella, J. A.; Huffman, J. C.; Caulton, K. G.; Longato, B.; Norton, J. R. *J. Am. Chem. Soc.* **1982**, *104*, 6360.
(21) Orpen, A. G.; Brammer, L.; Allen, F. H.; Kennard, O.; Watson, D. G.; Taylor, R. *J. Chem. Soc., Dalton Trans.* **1989**, S1.

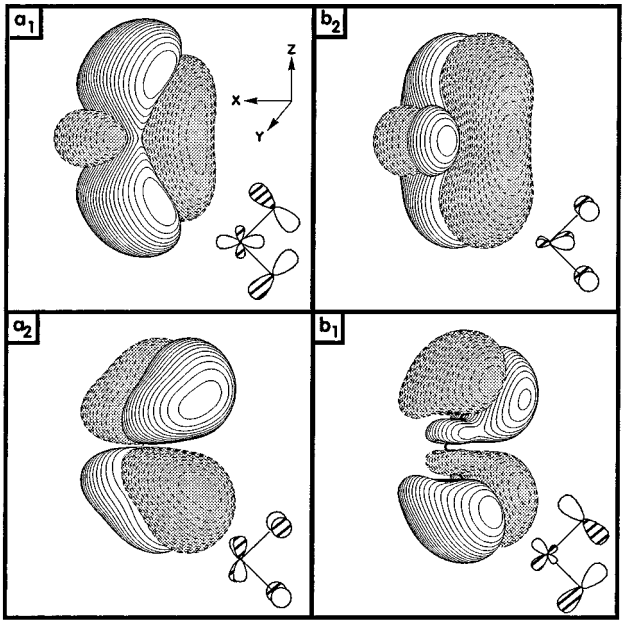

Figure 2. Three-dimensional contour plots of the π-orbitals of the $[(HO)_2Zr]^{2+}$ fragment in **9**.

bital, a_2 in Figure 2, is predominantly an out-of-phase combination of oxygen p_y-orbitals interacting in a bonding fashion with the zirconium d_{xy}-orbital. In this orbital the bent geometry of the fragment forces the oxygen atoms out of the *xy*-plane preventing optimal π-type overlap, resulting in a weak Zr−O π-interaction. (It would be maximal if the O−Zr−O angles were 180°, but recall that they are anywhere from 108° to 98.0° in **9**−**11**.) The next higher energy π-interaction, labeled b_2 in Figure 2, is largely an in-phase combination of oxygen p_y-orbitals mixing in a bonding fashion with a zirconium-centered dp-hybrid of largely d_{yz} character. The highest occupied fragment MO, labeled b_1 in Figure 2, is overwhelmingly an oxygen-centered MO composed of the out-of-phase combination of oxygen $(p_z + p_x)$-hybrid orbitals mixing in an essentially nonbonding fashion with a zirconium-based dp-hybrid that is largely d_{xz} in character. As in a_2 above, overlap in b_1 suffers from the bent geometry of the fragment. In this case the oxygen atoms are bent within the *xz*-plane so as to align the nodes of the oxygen p-orbitals almost directly along adjacent lobes of the dp-hybrid on the metal yielding little π-overlap. Thus two of the four Zr−O π-interactions are particularly weak, implying that the bishydroxide/bisalkoxide ligand set donates less electron density to a central metal atom than the bis-Cp ligand set does in the metallocene systems. Such a conclusion is not novel,[22] as those who regularly utilize dialkoxymetal fragments to mimic early metallocene systems anticipate increased electron deficiency at the metal.[23] Given this consideration, we believe that the Zr and W metal centers in **9**−**11**, along with their experimentally known analogues, are considerably more electron deficient than their corresponding metallocene counterparts.

(22) (a) Cai, S.; Hoffman, D. M.; Huffman, J. C.; Wierda, D. A.; Woo, H.-G. *Inorg. Chem.* **1987**, *26*, 3693. (b) Lin, Z.; Hall, M. B. *Coord. Chem. Rev.* **1993**, *123*, 149.

(23) See, for example: LaPointe, R. E.; Wolczanski, P. T.; Van Duyne, G. D. *Organometallics* **1985**, *4*, 1810.

While this analysis indicates a strong tendency for $(RO)_2M$ centers to seek η²-coordination, it fails to explain how the $(RO)_2M$ fragments containing group IV transition metals can accommodate two η²-bound ligands in the absence of empty, low lying f-orbitals. In their initial investigation of the metallocene−(η²-acyl) binding interaction Tatsumi, Nakamura, Hofmann, Stauffert, and Hoffmann[2b] noted that an acyl anion possesses two relatively high lying donor orbitals. The lower energy orbital, labeled n_+, is composed of an in-phase combination of an oxygen-centered p-orbital and a carbon-centered sp-hybrid that is strongly polarized toward the oxygen atom, as shown in **18** due to the greater electronegativity of oxygen. The higher energy orbital, labeled n_-, is the corresponding out-of-phase combination, polarized toward the carbon atom, as shown in **19**.

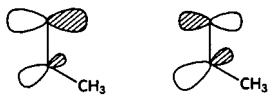

18 **19**

In the case of the mono(η²-acyl) complexes ($Cp_2M(\eta^2$-$COCH_3)R$), both of these donor MOs interact strongly with metallocene-centered fragment orbitals in which **18** serves in a σ-donor fashion and **19** serves in a π-donor fashion to the metal.[2b] Tatsumi, Nakamura, Hofmann, Hoffmann, Moloy, and Marks[3a] noted that of the four linear combinations of **18** and **19** derived from a coplanar bisacyl ligand set, only three found acceptor orbitals of suitable symmetry at the group IV metallocene center, rendering the bis-η²-acyl structure they examined unstable relative to $Cp_2M(\eta^2$-$COCH_3)(\eta^1$-$COCH_3)$. The critical interaction arose between the out-of-phase combination of **19** and a metal-centered dp-hybrid orbital as shown in **20**. In the coplanar geometry

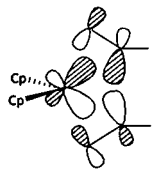

20

the positions adopted by the acyl ligands aligned the nodes of the acyl fragment orbitals directly along the principle lobes of the metal-centered dp-hybrid, resulting in little metal−ligand overlap. In the corresponding actinide metallocenes a metal-centered f-orbital mixes into the dp-hybrid in **20**, enhancing the metal−carbon bonding interaction while converting the metal−oxygen antibonding interaction in **20** into a bonding interaction with the appearance of two additional metal-centered lobes from the f-function. A most interesting aspect of the interaction in **20** is the carbon-centered nature of the acyl-based fragment orbitals, implying that if the bisacyl ligand set could adopt an alternative, noncoplanar geometry that would increase the metal−carbon bonding interaction in **20** while preserving the strength of the other three metal−acyl interactions, then it should be possible for a group IV metallocene center to bind two η²-bound ligands. We believe that the geometries exhibited by **9**−**11** do just this. By rotating about their coordination axes with the metal atoms, the

formyl, iminoformyl, and acetylene ligands in these species remove the antibonding interactions between the metal and the oxygen atoms in **20** while simultaneously increasing the C−M−C bond angle. This latter adjustment increases metal−carbon overlap, allowing the group IV $M(OR)_2$ moieties to bind two dihapto ligands (vida infra).

The Coupling Mechanism. Given the geometries of **9**−**11** (i.e., pseudotetrahedral geometry, head-to-tail alignment, C_2 symmetry) and the mechanistic proposals for acyl coupling in the actinide metallocene systems, two mechanistic pathways are obvious candidates for the coupling reactions in Scheme 2. The first of these involves a conrotatory motion of the η^2-bound ligands to generate a complex in which these ligands adopt a coplanar arrangement at the metal, analogous in structure to **1**, followed by in-plane carbon−carbon bond formation. As in the case of the actinide metallocene systems, this coupling mode was found to be symmetry forbidden.[24] This result prompted Rothwell and coworkers[24] to propose an alternative, least-motion pathway in which the η^2-bound ligands undergo a distortion that is most easily viewed as two separate motions, as highlighted in eq 4, that occur simultaneously. The first

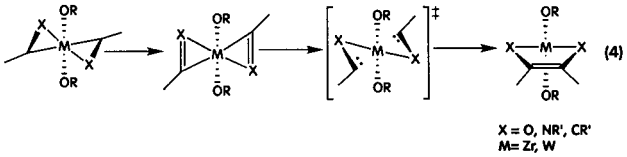

of these is a conrotation of the η^2-bound ligands about their coordination axes with the metal, which would, in a formal two-step mechanism, align the ligands parallel with the HO−M−OH plane as indicated in the first "step" of eq 4. The second process is a disrotatory motion of the C−X bond vectors that carries the carbon atoms away from the metal and toward one another in a scissors-like fashion, generating a transition state of C_2 symmetry that leads to the coupled product. Fundamentally, this pathway is little different from the mechanism proposed for η^2-acyl coupling in actinide metallocene complexes in Scheme 1. The only significant difference is the absence of an intermediate of C_{2v} symmetry (i.e., analogous to **1**). While we do not arbitrarily rule out such a structure, a least-motion pathway connecting a geometry of the type exhibited by **9**−**11** with the metallacyclic products does not require the appearance of a geometry bearing coplanar η^2-formyl, iminoformyl, or acetylene moieties.

To confirm that the pathway shown in eq 4 is symmetry allowed for our model compounds, we constructed Walsh diagrams for the coupling of the η^2-bound ligands in **9**−**11** in which C_2 symmetry is conserved throughout the process. The important valence regions for two of these diagrams are shown in Figure 3, where the one on the left, labeled A, corresponds to formyl coupling in **9** and the one on the right, labeled B, corresponds to acetylene coupling in **11**. The diagram for iminoacyl coupling in **10** closely follows that in A and is not shown. In both diagrams of Figure 3 the two highest occupied molecular orbitals, labeled 1a

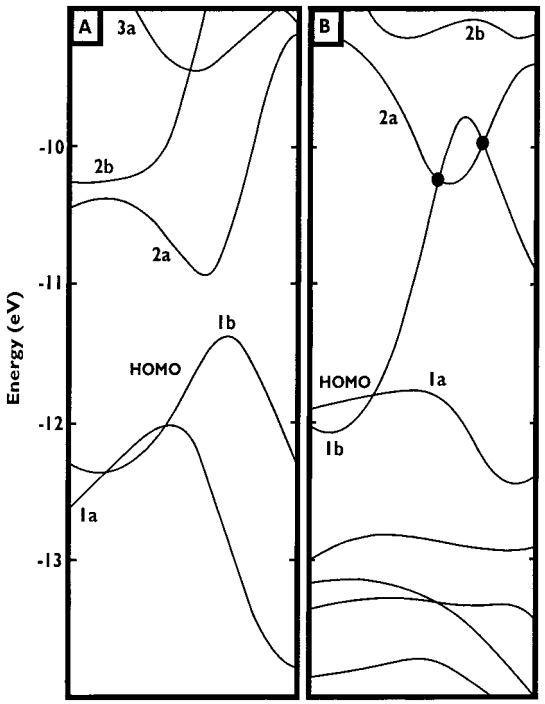

Figure 3. Walsh diagrams for the coupling of the formyl ligands in **9** (A) and the acetylene ligands in **11** (B).

and 1b, are the in-phase and out-of-phase (with respect to the C_2 axis) combinations of the ligand-centered n– (**19**) orbitals mixing in a bonding fashion with the metal. The two lowest unoccupied molecular orbitals, labeled 2a and 2b, are the in-phase and out-of-phase combinations of the ligand-centered π^* C−X (X = O, NH, CH) orbitals that lie perpendicular to the plane defined by the intraligand metal, carbon, and X atoms that contains the metal−ligand coordination axis. As the reaction proceeds, the 1a levels in both diagrams initially rise in energy until they undergo an avoided crossing with their 2a counterparts. This forces 1a down in energy, allowing it to correlate with a metallcycle π-orbital. The 1b levels behave similarly; after initially falling a bit in energy, they begin to rise rather rapidly in energy until they undergo avoided crossings with their 2b counterparts. The 1b levels fall back down in energy as they are transformed into the newly forming C−C π-bonds. Comparing the two Walsh diagrams in Figure 3 reveals that formyl coupling in **9** is formally symmetry allowed (as is iminoformyl coupling in **10**), whereas acetylene coupling in **11** is formally symmetry forbidden due to the far larger rise in energy of the 1b level in Figure 3B than in Figure 3A. Indeed, there is a gradual trend in the isoelectronic series **9**−**11** in which the 1b level rises higher in energy along the reaction coordinate as the electronegativity of the η^2-bound ligands decreases. Thus in the coupling of the formyl ligands in **9** the 1b level rises approximately 0.9 eV from its initial energy to its maximum energy along the reaction pathway, while the corresponding levels rise approximately 1.4 and 2.2 eV in the coupling of the iminoformyl ligands of **10** and the acetylene ligands of **11**, respectively. The origin of the energetic behavior of the 1b level is directly attributable to the electronegativity differences between O, N, and C in two ways. First, as the electronegativity of the η^2-bound ligands

(24) Durfee, L. D.; McMullen, A. K.; Rothwell, I. P. *J. Am. Chem. Soc.* **1988**, *110*, 1463.

decreases along the series formyl, iminoformyl, acetylene, the energies of the 2b levels in **9**−**11** lie at increasingly higher energies than those of the 1b levels. This results in an increasing 1b−2b energy gap along the series. As a result, the coupling between 1b and 2b diminishes as the ligand electronegativity decreases. So one would then expect that there will be an increasingly larger kinetic barrier as the electronegativity of the coupling ligands decreases. This same feature, namely, the size of the $n_- - \pi^*_{CX}$ energy gap, was noted by Hoffmann and co-workers[3a] as the critical factor in explaining why the carbamoyl ligands in $Cp^*_2An(\eta^2\text{-}CONMe_2)_2$ (An = U, Th) did not undergo ligand coupling to generate an enediamide complex when the corresponding acyl coupling occurs quite readily. In addition Rothwell and co-workers[24] have noted that altering the energy of the π^*_{CN}-orbitals in $(ArO)_2Zr(\eta^2\text{-}CR{=}NR')_2$ by changing the substituents on the iminoacyl nitrogen atoms changes the rate of ligand coupling in the expected fashion (i.e., π-donors decrease the reaction rate and π-acceptors increase the reaction rate). A critical factor in the **11** to **14** transformation is that the energy of 1b rises so high in energy that it crosses the 2a level, and the reaction becomes symmetry forbidden. We believe that there is a second way of explaining the energetic behavior of the 1b levels in **9**−**11** as a function of ligand electronegativity. The 1b level of **9**, shown as **21**, is composed of an out-of-phase combination of formyl

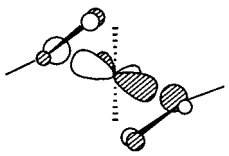

21

valence orbitals analogous to **19** mixing in a bonding fashion with a metal-centered dp-hybrid. Recall that this is exactly the same interaction that gave rise to the critical valence MO **20** that was found to be responsible for preventing the acyl ligands in the bisacyl complexes of the group IV metallocenes from attaining a coplanar arrangement. Note that from the perspective in **21** there is considerable bonding overlap between the carbon atoms of the η^2-bound ligands and the transition metal center that stabilizes the bis η^2-coordination geometry in **9**−**11**. Further examination of **21** shows the significant polarization of the ligand-based fragment orbitals that places more electron density onto the carbon atoms. As the formyl ligands in **9** couple by rotating in a conrotatory fashion, there is little energetic consequence as metal−carbon bonding is maintained. This behavior can be seen in the Walsh diagrams in Figure 3, where, in the beginning 1b actually falls in energy. Once the carbon atoms begin leaning away from the metal atom and toward one another, a considerable amount of metal−carbon bonding overlap is lost, causing 1b to rise in energy until the stabilization associated with carbon−carbon bond formation forces the 1b level back down. It is then the relative timing of these two events that determines how high 1b rises along the reaction path. In the case of **9**, where the ligand-centered orbitals are strongly polarized onto the carbon atoms, little metal−carbon bonding overlap is lost prior to carbon−carbon bond formation, resulting in a relatively small rise in the energy of the 1b level. In **10**, where there is less polarization of the ligand-centered fragment orbitals, and in **11**, where polarization of the acetylene-centered fragment orbitals is nonexistent, little metal−carbon bonding overlap is retained, forcing the 1b level to rise higher in energy.

Assuming that this trend in the behavior of the 1b level is responsible for the relative kinetic profiles for the three coupling reactions in Figure 1, we can conclude that the rates at which coupling occurs should be in the order **9** > **10** > **11**. Such an ordering would nicely match the trend noted by Rothwell and co-workers[5,7] in which no bis-η^2-ligated intermediate could be observed in the formation of eneamidolate **6**, whereas bis-η^2-iminoacyl complex **4** could be isolated and undergoes iminoacyl coupling rather easily, and the bis-η^2-acetylene complex **7** required forcing conditions to generate tungstacyclopentatriene **8**. This prompted us to undertake transition state searches for each of the three model reactions at the B3LYP level of theory. The resulting reaction profiles for formyl coupling in **9** and iminoformyl coupling in **10** are shown in Figures 4A and 4B, respectively, along with transition state and product structures (vida infra). Numerous attempts at locating a transition state for acetylene coupling in **11** were unsuccessful, presumably due to the orbital crossing shown in Figure 3B. As can be seen in Figure 4A, transition state **22** connecting **9** with **12** occurs quite late along the reaction coordinate. The formyl carbon atoms have pivoted away from the zirconium atom, approaching a coplanar arrangement associated with metallacycle formation, and the newly forming carbon−carbon bond is well along the way to completion (2.11 Å). The zirconium−oxygen bonds are shortened by approximately 0.17 Å from their corresponding values in **9**, indicating that the conversion from dative Zr−O interactions to full σ-bonds is essentially halfway completed. We were surprised to see that the Zr−C distances in **22** were 0.01 Å *shorter* than the Zr−C bond length in **9**, which initially seemed to indicate that zirconium−carbon bonding character *increased* as transition state **22** is reached. However, examination of reduced overlap populations obtained from extended Hückel calculations of the B3LYP-optimized geometries of **9** and **22** showed that zirconium−carbon bonding character is reduced by ∼25% in the transition state. This indicated to us that the short Zr−C distances in **22** are a reflection of the geometrically tight transition state structure and as a result are surprisingly insensitive indicators of how much zirconium−carbon bonding character is retained at the transition state. It is interesting to note that the carbon atoms of **22** possess considerable singlet methylene character, with sp^2-like O−C−H bond angles of 115.8°. This is also reflected in the reaction trajectory taken by the carbon atoms as they approach one another with their O−C−H planes aligned in a parallel fashion, which strongly resembles the reaction trajectory calculated for the dimerization of singlet methylene.[25] This carbenoid nature of the coupling process in **9** agrees with a number of early mechanistic proposals[1d,e] for the coupling of acyl ligands in metallocene complexes.

(25) Hoffmann, R.; Gleiter, R.; Mallory, F. B. *J. Am. Chem. Soc.* **1970**, *92*, 1460.

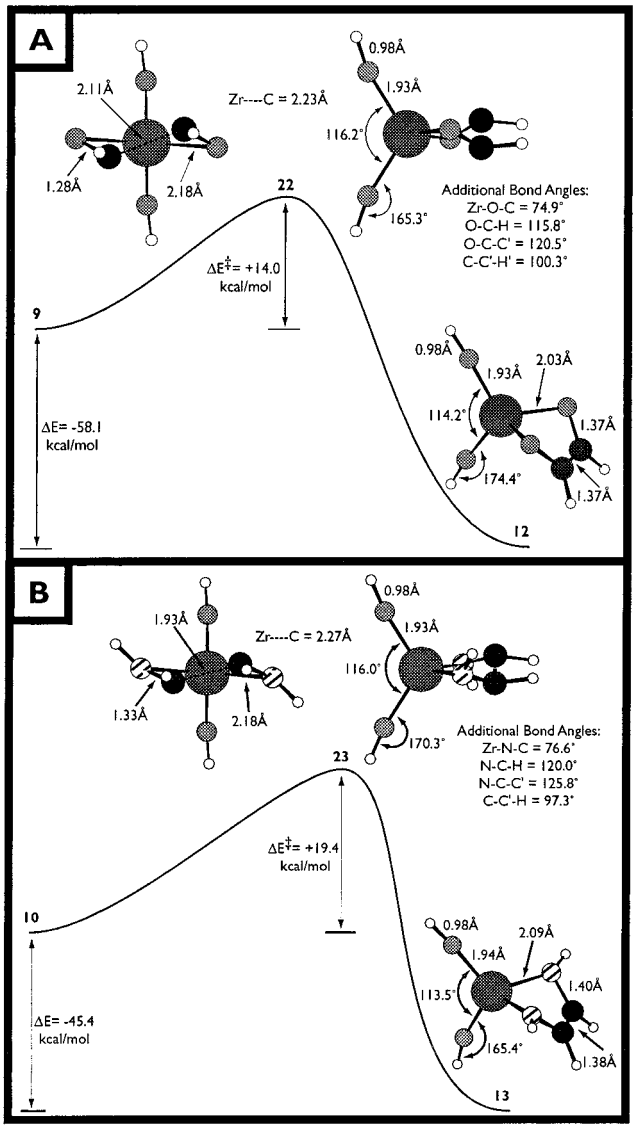

Figure 4. Reaction profiles of formyl coupling in **9** (A) and iminoacyl coupling in **10** (B) along with the B3LYP-optimized geometries of the corresponding transition states and products.

The same general characteristics are seen in transition state **23**, which connects **10** with **13** in Figure 4B. Again, the transition state occurs quite late along the reaction coordinate. Carbon−carbon bond formation has progressed to a larger extent in **23**, as indicated by the 1.93 Å carbon−carbon bond length, which is 0.08 Å shorter than the corresponding value in **22**. The zirconium−nitrogen bond lengths of 2.18 Å are 0.15 Å shorter than the corresponding bond lengths in **10**, indicating that the conversion of the dative Zr−N bonds in **10** to full σ-bonds is considerably more than halfway completed. Inspection of the Zr−C reduced overlap populations calculated at the extended Hückel level using the B3LYP-optimized geometries of **10** and **23** reveals the loss of ∼45% of the zirconium−carbon bonding character originally present in **10**, which is nearly twice as much as is lost in the coupling of the formyl ligands in **9**. This served to further confirm our initial belief that the reactivity differences observed by Rothwell and co-workers arise from differences in the electronegativity of the η^2-bound ligands. The same singlet carbenoid character we observed at the carbon atoms in **22** is also present at the carbon atoms of **23**, where the N−C−H bond angle measures 120.0°. Finally, in both **22** and **23** the significant bonding changes undergone by the η^2-bound ligands scarcely perturb the geometry of the $Zr(OH)_2$ moiety, with the only significant difference being an increase of ∼8−12° in the HO−Zr−OH bond angle in both systems.

As our extended Hückel calculations predicted, the kinetic barrier to formyl coupling in **9** of 16.8 kcal/mol is approximately 5.4 kcal/mol smaller than the kinetic barrier to iminoformyl coupling in **10** at the B3LYP level of theory. While no experimental measurement for formyl coupling exists, Rothwell and co-workers have undertaken kinetics measurements for the coupling in a number of bis(η^2-iminoacyl) complexes.[24] The 19.4 kcal/mol barrier we calculated for iminoformyl coupling (Figure 4B) compares well with the measured $\Delta H^{\ddagger}$ values (21.0−27.7 kcal/mol) Rothwell obtained.

The Enediolate, Enediamide, and Tungstacyclopentatriene Products. Rothwell and co-workers[26] have noted that the chelating X−CH=CH−X (X = O, NH) ligands appearing in **12** and **13** are members of a family of bidentate chelates, all of which are isoelectronic with butadiene and as such can be described as some combination of two limiting resonance structures[26] (**24** and **25**) analogous to those used to describe the

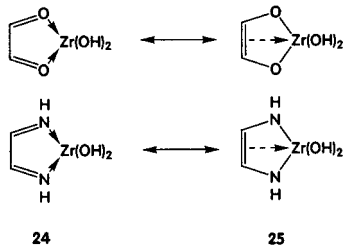

electronic structure of η^4-butadiene complexes of the transition metals.[1a] In resonance structure **24** the chelating ligands are viewed as neutral, four-electron donors bound to the metal by a pair of dative Zr−X (X = O, NH) interactions, whereas in resonance structure **25**, the ligands are doubly reduced by the metal to generate the dianionic enediolate and enediamide moieties. Readers familiar with the geometric trend observed in η^4-butadiene complexes will recognize **24** as a modified form of the π^2-binding mode observed in late transition metal complexes and **25** as reminiscent of the $\sigma^2\pi$ binding mode found in the butadiene complexes of the early transition metals. Given the propensity of group IV transition metals to achieve the +4 oxidation state, it is no surprise that our optimized geometry of **12** (C_s symmetry), shown in Figure 4A, closely resembles resonance form **25** with C−O bonds (1.37 Å) that are anywhere from 0.11 to 0.18 Å longer than a typical carbonyl C=O bond[26−28] and a C=C bond length of 1.37 Å, which is only 0.05 Å longer than the C=C bond in ethylene.[27] At 2.03 Å the endocyclic Zr−O bonds are far

(26) Chamberlain, L. R.; Durfee, L. D.; Fanwick, P. E.; Kobriger, L. M.; Latesky, S. L.; McMullen, A. K.; Steffey, B. D.; Rothwell, I. P.; Folting, K.; Huffman, J. C. *J. Am. Chem. Soc.* **1987**, *109*, 6068.

(27) March, J. *Advanced Organic Chemistry: Reactions, Mechanisms, and Structure*, 4th ed.; Wiley: New York, 1992.

(28) Allen, F. H.; Kennard, O.; Watson, D. G.; Brammer, L.; Orpen, A. G.; Taylor, R. *J. Chem. Soc., Perkin Trans. 2* **1987**, S1.

shorter than the 2.20−2.40 Å distances typically observed[21] for the dative Zr−O interaction in tetrahydrofuran complexes of zirconium, indicating the presence of a formal σ-bond. The most interesting structural feature of **12** is the envelope-folded conformation exhibited by the zirconacycle that pushes the carbon atoms out of the endocyclic O−Zr−O plane by 50.7°. As a result of this distortion, the olefinic C═C bond of the zirconacycle is π-bound to the central zirconium atom with Zr−C bond lengths of 2.51 Å, which compares very favorably with the mean Zr−C_{Cp} bond length of 2.53 Å observed in Cp_2Zr fragments.[21,26] Thus **12** exhibits the same $\sigma^2\pi$-coordination geometry observed in the early transition metal complexes of butadiene.[29] In fact this envelope-folded conformation has been observed in nearly all complexes of the form $Cp_2M[X-CR=CR-X]$ (M = Ti, Zr, Hf; X = O, S, Se, Te, NH).[30] Our calculated structure of **12** compares well particularly with respect to the Zr−O and C−O bond distances to $Cp^*_2Zr[O-C(CH_3)=C(CH_3)-O]$ and $Cp^*_2Zr[O-C(^tBu)=C(^tBu)-O]$, which are to our knowledge the only known mononuclear enediolate complexes of zirconium to be characterized crystallographically.[31]

The B3LYP-optimized geometry of **13** (C_s symmetry), shown in Figure 4B, possesses many of the same general structural characteristics as **12**, including a distinct resemblance with resonance form **25** above. This is confirmed by comparing the calculated 1.40 Å C−N and 1.38 Å C−C bond lengths in **13** with the 1.257(6) Å C−N and 1.457(2) Å C−C bond lengths observed in 1,4-dicyclohexyl-1,4-diazabutadiene.[26,32] At 2.09 Å the Zr−N bond lengths in **13** fall into the range typically reserved for zirconium−amido interactions.[21] The zirconacycle in **13** exhibits the same envelope-folded conformation that we found in **12**, with the olefinic moiety of the zirconacycle pushed out of the N−Zr−N plane by 50.0°. As a result, the olefinic carbon atoms sit 2.59 Å away from the zirconium atom, which once again implies that the C═C bond is formally coordinated to Zr. Our calculated geometry of **13** compares quite well with the experimentally observed structure[26] of $(2,6\text{-}(^tBu)_2PhO)_2Zr[(2,6\text{-}(CH_3)_2Ph)N-C(CH_3)=C(CH_3)\text{-}N(2,6\text{-}(CH_3)_2Ph)]$, which exhibits Zr−N bonds of 2.06 Å, C−N bonds of 1.43 Å, and a C═C bond measuring 1.37 Å. Coupling of the acetylene ligands in **11** results in the formation of tungstacyclopentatriene **14**, which is shown in Figure 5 along with important bond distances and angles. This species also exhibits many of the same structural characteristics that we found in **12**, including the presence of a metallacycle that closely resembles limiting resonance structure **25** with one exception, namely, that at 1.93 Å, the W−C_α bonds are 0.21 Å shorter than the W−CH_3 linkage observed in WMe_6 [33] and are ∼0.30 Å shorter than the mean W−C_{alkyl} bond distance reported in a survey[21] of metal−ligand interactions compiled from the structures present in the Cambridge Crystallographic Database. This indicates the presence of considerable W−C_α multiple-bond character, which is confirmed by the fact that these W−C_α bond lengths fall squarely in the middle of the range spanned by tungsten−alkylidene linkages.[34] The $C_\alpha-C_\beta$ and $C_\beta-C_{\beta'}$ bond lengths are equivalent to one another at 1.42 Å, also indicating considerable delocalization of the electron density within the tungstacycle. Furthermore **14** exhibits the same envelope-folded conformation present in **12** and **13**, with the C_β and $C_{\beta'}$ atoms bent out of the $C_\alpha-W-C_\alpha$ plane by 54.8°. This places the $C_\beta/C_{\beta'}$ atoms 2.41 Å from the tungsten atom, which is within 0.08 Å of the mean 2.33 Å W−C_{Cp} distance observed in (η^5-C_5H_5)-W π-type interactions.[21] Our calculated structure of **14** compares quite favorably to the experimentally observed[7] geometry of $[(2,6\text{-}Ph_2C_6H_3)O]_2W[C_4(C_2H_5)_4]$, **8**.

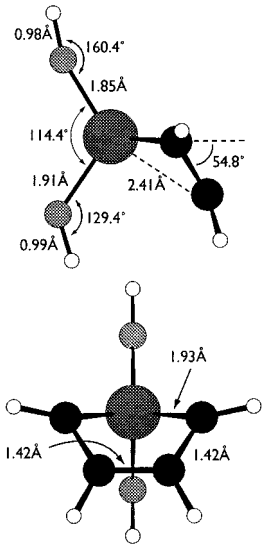

Figure 5. B3LYP-optimized geometry of tungstacyclopentatriene complex **14**.

Thermodynamically, all three of these ligand coupling processes are extremely exothermic, with the formation of enediolate **12** releasing 58.1 kcal/mol (Figure 4A), the formation of enediamide **13** releasing 45.4 kcal/mol (Figure 4B), and the formation of tungstacyclopentatriene **14** releasing 21.4 kcal/mol. Attempting to rationalize the magnitudes of these ΔE values is not warranted due to the dearth of accurate bond dissociation energies available to model the metal−ligand interactions in **12**−**14**. However, when we consider that the coupling reactions all result in the formation of a new C═C bond (BDE = 172 kcal/mol),[35] it seems reasonable to anticipate an overall exothermic process in all three cases. In addition, the conversions of **9** to **12** and **10** to **13** receive additional thermodynamic assistance from the formation of strong Zr−O and Zr−N σ-bonds at the expense of the corresponding, relatively weak dative interactions in **9** and **10**.

Rothwell and co-workers noted[7a,26] that the metallacycles are fluxional species that interconvert between

(29) (a) Yasuda, H.; Tatsumi, K.; Nakamura, A. *Acc. Chem. Res.* **1985**, *18*, 120. (b) Collman, J. P.; Hegedus, L. S.; Norton, J. R.; Finke, R. G. *Principles and Applications of Organotransition Metal Chemistry*; University Science Books: Mill Valley, CA, 1987.

(30) Hey-Hawkins, E. *Chem. Rev.* **1994**, *94*, 1661.

(31) Hofmann, P.; Frede, M.; Stauffert, P.; Lasser, W.; Thewalt, U. *Angew. Chem., Int. Ed. Engl.* **1985**, *24*, 712.

(32) Van Koten, G.; Vrieze, K. *Adv. Organomet. Chem.* **1982**, *21*, 153.

(33) Haaland, A.; Hammel, A.; Rypdal, K.; Volden, H. V. *J. Am. Chem. Soc.* **1990**, *112*, 4547.

(34) Winter, M. J.; Woodward, S. In *Comprehensive Organometallic Chemistry II*; Abel, E. W., Stone, F. G. A., Wilkinson, G., Eds.; Pergamon: Tarrytown, NY, 1995; Vol. 5, Chapter 5.

(35) *Handbook of Chemistry and Physics*, 71st ed.; Lide, D. R., Ed.; CRC Press: Boca Raton, FL, 1990.

two equivalent conformations, presumably via transition states of C_{2v} symmetry, as shown in reaction 5. Furthermore, using variable-temperature NMR, they found that the rates of this inversion process follow the order **6** > **5** > **8**. The inversion of eneamidolate complexes (**6**) could not be slowed sufficiently to observe line broadening in a ^{1}H NMR spectrum at −75 °C, whereas the activation energies of the ring inversion in a number of enediamide complexes (**7**) could be measured ($\Delta H^{\ddagger}$ = 12.7−15.5 kcal/mol). Tungstacyclopentatriene **8** inverted so slowly that its kinetic barrier could only be estimated as being >18 kcal/mol. Given the relatively high symmetry of the flat metallacycles (C_{2v}), we undertook transition state searches for the ring inversions in **12**−**14** at the B3LYP level. The geometries of the resulting structures are unremarkable. Most importantly we found that inversion of the enediolate ring in **12** possesses the smallest barrier, at 6.5 kcal/mol, followed by inversion of the enediamide ring in **13**, with an inversion barrier of 12.2 kcal/mol, and inversion of the tungstacyclopentatriene ring in **14**, with a barrier of 35.2 kcal/mol. Hofmann and co-workers[31] demonstrated that the electronic driving force associated with metallacycle bending in the zirconocene enediolates **24** and **25** was the donor/acceptor interaction arising between the frontier MOs of the flat metallacycle, namely, the mixing between the filled olefinic π-bond and the lowest unoccupied MO, an empty metal d-orbital. As the metallacycle bends, these two orbitals mix into one another, stabilizing the HOMO and destabilizing the LUMO to generate an increased HOMO/LUMO gap. As the electronegativity of X increases from C to N to O, the HOMO of the flat metallacycle decreases in energy. Since the metal-centered LUMO is left essentially unchanged by this perturbation, the HOMO−LUMO gap widens, reducing the magnitude of this interaction and consequently the degree to which the HOMO is stabilized by metallacycle folding. Thus, assuming that the flat metallacyclic structure is the transition state for ring inversion, those metallacycles containing more electronegative X-moieties should possess smaller kinetic barriers to ring inversion because the HOMO rises less in energy upon passing from 1-folded conformation to the transition state. The extraordinarily large value associated with tungstacycle inversion in **14** is not a true kinetic barrier, as the flat tungstacycle possessing C_{2v} symmetry is a third-order saddle point, indicating that if ring inversion occurs in this complex, it must do so by some more complicated mechanism.

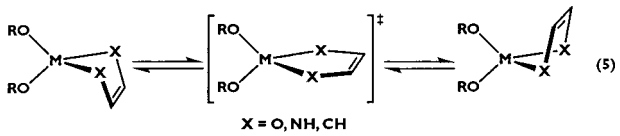

(5)

Conclusions

The results of Rothwell and co-workers describing the ability of the $[(RO)_2M]^{2+}$ (M = Ti, Zr, Hf, W) metal fragment to bind two iminoacyl or acetylene ligands in an η^2-fashion was a bit surprising given that the corresponding isolobal $[Cp_2M]^{2+}$ fragment is commonly believed to be unable to do so, as it would generate a thermodynamically unstable 20-valence-electron complex. We have found using MO calculations at the hybrid DFT level that the $[(RO)_2M]^{2+}$ fragment is not as close to being a $[Cp_2M]^{2+}$ equivalent as one might initially believe because the metal−alkoxide interactions possess considerably less multiple-bond character. Our calculations show that of the four possible π-interactions between the metal and the alkoxide ligands, two are weaker due to poor metal−oxygen π-overlap caused by the bent geometry of $[(RO)_2M]^{2+}$. This makes each alkoxide ligand an effective four-electron donor, leaving the central metal atom in $[(RO)_2M]^{2+}$ more electron deficient than that in $[Cp_2M]^{2+}$. We have also examined how the progressive decrease in electronegativity of the η^2-bound ligands in the isoelectronic series $(HO)_2Zr(\eta^2\text{-}CHO)_2$, **9**, $(HO)_2Zr(\eta^2\text{-}HNCH)_2$, **10**, and $(HO)_2W(\eta^2\text{-}HCCH)_2$, **11**, affects the rate at which the ligands couple via a single-step mechanism to generate enediolate complex **12**, enediamide complex **13**, and tungstacyclopentatriene **14**. We have found a general increase in the kinetic barriers to ligand coupling as the electronegativity of the η^2-bound ligands decrease, which agrees with experimental observations in closely related systems. We have attributed this trend in kinetic barriers to the behavior of a filled, high lying MO, labeled 1b, that is affected in two ways by the progressive shift in electronegativity of the η^2-bound ligands in the series **9**−**11**. In all three cases this orbital undergoes an avoided crossing with a higher lying, empty π^*_{CX}-orbital. As the electronegativity of the ligand set decreases, the energy gap between the 1b level and the empty π^* MO increases. This allows 1b to rise increasingly higher in energy before the stabilization associated with the avoided crossing occurs, resulting in progressively larger kinetic barriers as ligand electronegativity decreases. In addition, the composition and nature of the 1b MO as it evolves along the reaction coordinate shows that its energy will be sensitive to the electronegativity of the atoms connected to the metal. Our calculations show all three reactions to be strongly exothermic.

Acknowledgment. We wish to thank the Robert A. Welch Foundation for generous support of this work.

OM000064I